

Contract No:

This document was prepared in conjunction with work accomplished under Contract No. DE-AC09-08SR22470 with the U.S. Department of Energy.

Disclaimer:

This work was prepared under an agreement with and funded by the U.S. Government. Neither the U. S. Government or its employees, nor any of its contractors, subcontractors or their employees, makes any express or implied: 1. warranty or assumes any legal liability for the accuracy, completeness, or for the use or results of such use of any information, product, or process disclosed; or 2. representation that such use or results of such use would not infringe privately owned rights; or 3. endorsement or recommendation of any specifically identified commercial product, process, or service. Any views and opinions of authors expressed in this work do not necessarily state or reflect those of the United States Government, or its contractors, or subcontractors.

THE IMPACT OF DISSOLVED SALTS ON PASTES CONTAINING FLY ASH, CEMENT AND SLAG

John R. Harbour, T. B. Edwards and V. J. Williams
Savannah River National Laboratory

ABSTRACT

The degree of hydration of a mixture of cementitious materials (Class F fly ash, blast furnace slag and portland cement) in highly concentrated alkaline salt solutions is enhanced by the addition of aluminate to the salt solution. This increase in the degree of hydration, as monitored with isothermal calorimetry, leads to higher values of dynamic Young's modulus and compressive strength and lower values of total porosity. This enhancement in performance properties of these cementitious waste forms by increased hydration is beneficial to the retention of the radionuclides that are also present in the salt solution. The aluminate ions in the solution act first to retard the set time of the mix but then enhance the hydration reactions following the induction period. In fact, the aluminate ions increase the degree of hydration by ~35 % over the degree of hydration for the same mix with a lower aluminate concentration. An increase in the blast furnace slag concentration and a decrease in the water to cementitious materials ratio produced mixes with higher values of Young's modulus and lower values of total porosity. Therefore, these operational factors can be fine tuned to enhance performance properties of cementitious waste form.

Empirical models for Young' modulus, heat of hydration and total porosity were developed to predict the values of these properties. These linear models used only statistically significant compositional and operational factors and provided insight into those factors that control these properties.

KEY WORDS: Calorimetry (A), Hydration (A), Rheology (A), Elastic Moduli (C), Alkali Activated Cement (D), Fly Ash (D), Granulated Blast-Furnace Slag (D), Cement (D)

DISCLAIMER

This work was prepared under an agreement with and funded by the U.S. Government. Neither the U.S. Government or its employees, nor any of its contractors, subcontractors or their employees, makes any express or implied: 1. warranty or assumes any legal liability for the accuracy, completeness, or for the use or results of such use of any information, product, or process disclosed; or 2. representation that such use or results of such use would not infringe privately owned rights; or 3. endorsement or recommendation of any specifically identified commercial product, process, or service. Any views and opinions of authors expressed in this work do not necessarily state or reflect those of the United States Government, or its contractors, or subcontractors.

1.0 INTRODUCTION

Savannah River Site (SRS) immobilizes low levels of radionuclides present in concentrated alkaline salt solutions by incorporating the radioactive salt solutions within a cementitious waste form [1-2]. At the Saltstone Production Facility (SPF), the alkaline salt solution is combined with premix (a mixture of 10 wt % portland cement (PC), 45 wt % blast furnace slag (BFS) and 45 wt % Class F fly ash (FA)) using a Readco mixer to produce a fresh (uncured) paste that is referred to as Saltstone. This paste contains no aggregate and has rheological properties that produce a self-consolidating and free flowing mix that can be pumped through a 3-inch line to disposal vaults. Once the paste has cured, the grout must exhibit performance properties that make it acceptable as a waste form within the vaults to limit leaching of the radionuclides into the environment. Both the type and concentration of dissolved salts in the aqueous solution have a significant impact on the processing and performance properties of the grout. This report presents data to demonstrate the impact of these dissolved salts on the properties of the Saltstone waste forms.

The premix composition along with the high salt and high free hydroxide ion concentrations leads to a complex system of reactions and interactions. The PC hydrates normally in this system to produce calcium silicate hydrate (CSH) [3-4]. Alkali activation of the BFS is well known and with the relatively high concentration of calcium in the slag, the product of these hydration reactions is also CSH [5-9]. The FA, with its low calcium content (0.11 wt % CaO), is activated by hydroxide ions to generate sodium aluminosilicates. This reaction is the basis of one type of geopolymer although in practice the properties of the geopolymers are generally enhanced by increasing the curing temperature to a value between 60 and 90 °C [10-11].

A new process has been introduced at the SRS as part of the disposition of radioactive waste streams. This new process is a pretreatment of the High Level Waste (HLW) sludge using caustic leaching to remove aluminum from the HLW sludge prior to sending this feed stream for vitrification at the Defense Waste Processing Facility (DWPF) [12]. The strategy here is to reduce the amount of HLW and the overall cost for treatment and disposition. The aluminate rich leachate is combined with other low activity radioactive waste streams to be incorporated into Saltstone at the SPF. It turns out that aluminate ions in the liquid phase can significantly impact the properties of pastes [13-14] and consequently further complicate the paste chemistry. Therefore, in this report aluminate concentration is addressed as a key driver of the paste properties.

2.0 EXPERIMENTAL

2.1 Materials

The cementitious materials were obtained from the SPF in sealed 5-gallon containers (Table 2-1). These materials were specified in a contract for SPF cementitious materials and arrived with the delivery of the cementitious materials to SPF. The materials were transferred to smaller high-density polyethylene bottles and tightly sealed. Table 2-1 also contains the wt% contribution of each material used to make the nominal premix. The fly ash used in this study was a Class F fly ash that was obtained from SEFA after it had been thermally treated by SEFA to remove most of the carbon and ammonia (referred to as carbon burnout or CBO fly ash). The

chemical compositions of the cementitious materials used in this study are presented in Table 2-2.

Table 2-1 Saltstone Cementitious Materials and Nominal Premix Blend

Material	Category	Vendor	Premix Blend (wt%)
Portland cement (PC)	Type II	Holcim	10
Blast Furnace slag (GGBFS)	Grade I	Holcim	45
Fly ash (FA)	Class F	SEFA	45

Table 2-2 Chemical Compositions of Saltstone Cementitious Materials (wt %)

OXIDE	OPC (%)	BFS (%)	FA (%)
Al ₂ O ₃	5.4	8.4	26.3
CaO	64.9	38.5	1.1
Fe ₂ O ₃	3.7	0.4	7.4
K ₂ O	0.5	0.3	2.9
MgO	1.2	12.9	1.1
Na ₂ O	0.1	0.3	0.4
SO ₄	3.2	1.0	0.1
SiO ₂	20.5	37.9	53.3
TiO ₂	0.3	0.4	1.3

Two types of salt solution simulants were used for this study. The first type was a Modular Caustic side solvent extraction Unit (MCU) simulant and the second simulant was a Salt Waste Processing Facility (SWPF) simulant both of which were based on projections of the expected compositions of the salt solutions after pretreatment by these two methods of solvent extraction. Initially, the simulants were projected to have relatively low levels of aluminate (Al(OH)₄⁻) as shown in Table 2-3. The inclusion of an aluminum removal step for HLW sludge and new projections based on more recent analyses of the tank salt solutions have increased the projected levels of aluminate in the salt solutions. The increase in aluminate has been addressed by varying the aluminate concentration in the simulants and also in the experimental designs provided in Section 2.2.

Table 2-3 MCU and SWPF Simulants at Low Levels of Aluminate

Low Aluminate Simulants	MCU Simulant	SWPF Simulant
Compound	(M)	(M)
NaOH	1.377	2.409
NaNO ₃	3.159	2.316
NaNO ₂	0.368	0.484
Na ₂ CO ₃	0.176	0.118
Na ₂ SO ₄	0.059	0.055
Al(NO ₃) ₃	0.054	0.114
Na ₃ (PO ₄)	0.012	0.007
Total Na Molarity	5.41	5.57

2.2 Experimental Design

Phase 1 and 2 of this study used simulants based on SWPF salt streams (Tables 2-4 and 2-5 respectively). In the phase 1 design, variation was introduced in the concentrations of total nitrate plus nitrite, free hydroxide and aluminate concentrations, w/cm ratio and wt % BFS. The mixes identified as GVS87 and GVS96 in phase 1 were replicate runs of the center point of the design. Phase 2 maintained a constant simulant and introduced variation in the water to cementitious materials (w/cm) ratio over the range of 0.50 to 0.65 in 0.05 increments at 2 levels of slag content (45 wt % and 60 wt %). GVS97 and GVS106 were mixes batched with higher portland cement content at the expense of the CBO FA.

Table 2-4 Design for Phase 1 of the Saltstone Variability Study

Design of Phase 1							
Identifier	Water/Premix	Cement	Fly Ash	Slag	Free OH	Nitrate plus Nitrite	Aluminate
	Ratio	Wt %	Wt %	Wt %	Molarity	Molarity	Molarity
GVS87	0.55	10.0	37.5	52.5	2.41	2.80	0.2816
GVS88	0.60	10.0	45.0	45.0	1.91	3.30	0.1144
GVS89	0.50	10.0	45.0	45.0	2.91	3.30	0.1144
GVS90	0.60	10.0	30.0	60.0	2.91	2.30	0.1144
GVS91	0.50	10.0	45.0	45.0	2.91	2.30	0.4488
GVS92	0.50	10.0	30.0	60.0	1.91	2.30	0.1144
GVS93	0.60	10.0	30.0	60.0	2.91	3.30	0.4488
GVS94	0.60	10.0	45.0	45.0	1.91	2.30	0.4488
GVS95	0.50	10.0	30.0	60.0	1.91	3.30	0.4488
GVS96	0.55	10.0	37.5	52.5	2.41	2.80	0.2816

Table 2-5 Design for Phase 2 of the Saltstone Variability Study

Design of Phase 2							
Identifier	Water/Premix	Cement	Fly Ash	Slag	Free OH	Nitrate plus Nitrite	Aluminate
	Ratio	Wt %	Wt %	Wt %	Molarity	Molarity	Molarity
GVS97	0.575	15	40	45	2.41	2.457	0.2816
GVS98	0.50	10	45	45	2.41	2.457	0.2816
GVS99	0.55	10	45	45	2.41	2.457	0.2816
GVS100	0.60	10	45	45	2.41	2.457	0.2816
GVS101	0.65	10	45	45	2.41	2.457	0.2816
GVS102	0.50	10	30	60	2.41	2.457	0.2816
GVS103	0.55	10	30	60	2.41	2.457	0.2816
GVS104	0.60	10	30	60	2.41	2.457	0.2816
GVS105	0.65	10	30	60	2.41	2.457	0.2816
GVS106	0.575	20	35	45	2.41	2.457	0.2816

2.3 Measurement of Properties

The measurements of processing and performance properties are described in this Section.

Rheology Rheological properties were determined using a Haake M5/RV30 rotoviscometer. The flow curves for the mixes were fitted to the Bingham Plastic rheological model to determine the yield stress (Pa), and the plastic viscosity (Pa s) [15].

Set Times A Vicat Consistency Tester was used to measure the final set times at a frequency (resolution) of one day.

Bleed Fresh paste was poured into cylinders of dimensions of 3.3 cm in diameter and 8.5 cm in height. These cylinders were capped and the volume of bleed measured after 24 hours. The tests were done in duplicate and the average of these two results was presented in units of volume % bleed liquid.

Fresh Density The density of the fresh paste was measured using a BYK-Gardner cup with a capacity of 8.32 g of water at 25 °C.

Compressive Strength For compressive strength measurements, the samples were cast in 2 x 4 inch cylinders, capped, taped and then allowed to cure for 28 days at ambient temperature prior to de-molding and measurement. Samples were batched and measured in triplicate for this unconfined compressive strength measurement.

X-Ray Diffraction (XRD) A Siemens Model D500 automated Scanning Diffractometer was used to evaluate the powders for evidence of crystallites within the cured pastes.

Heat of Hydration The heat of hydration measurements were performed using a TAM Air Isothermal Calorimeter, Model Number 3116 that was manufactured in Sweden and distributed by TA Instruments. The calorimeter consists of 8 channels with each channel comprised of both

a sample and reference port. This allows for eight different samples to be measured simultaneously at a given temperature. After the three minute mixing period, ~ 8 mL of the mix were transferred to the sample vial which was then weighed and placed within the calorimeter. The equilibration time after placement of the sample in the calorimeter was typically 45 minutes prior to data acquisition.

Scanning Electron Microscopy (SEM) Electron microscopy of samples was carried out at Clemson University's Advanced Materials Research Laboratory using an Hitachi S3400 Variable Pressure SEM equipped with Energy dispersive X-ray (EDS) for elemental analyses. In some cases samples were polished and backscattered electron (BSE) images recorded. Secondary electron images were also obtained.

Dynamic Young's Modulus (E) The dynamic Young's Modulus (E) was measured according to ASTM C 215-02 using an E-Meter Mk II Resonant Frequency Tester by James Instruments Inc. The method involves a longitudinal impact on the end of a 3 x 6 inch cylinder of cast and cured paste, detection of the sound waves produced at the opposite end of the cylinder, and measurement of the fundamental resonance frequency of the cylinder through a fast Fourier transform of the time domain signal. Using this resonance frequency and the independently measured mass and dimensions of the cylinder, the dynamic Young's modulus was calculated as discussed in ASTM C 215.

Total Porosity (Φ) The porosity was determined by the mass loss upon heating samples (1.5 to 2 grams) to 105 °C using a Mettler Toledo HR83 Moisture Analyzer. The cured paste pieces that were used in the measurement of porosity were taken from the center of the cylinder by breaking the cylinder and removing pieces from the central region. The total porosity of a cured sample of portland cement in water at 0.60 w/c ratio was measured by this technique and gave a value of 48 % which is consistent with the porosity reported in the literature for this mix [9]. Additional confirmation of this method for salt simulant pastes was performed using a Netzsch STA 409 PC thermal analyzer to measure the mass change with temperature up to ~ 800 °C. Finally, the total porosities were corrected for the inclusion of salt within the pore liquid which remains within the pores of the paste after heating to 105 °C.

3.0 RESULTS AND DISCUSSION

The results presented in this report were measured from mixes batched with either MCU or SWPF simulated salt solutions and in some cases, NaOH solutions. The major focus of this report is on the performance properties of the cured pastes and the factors that influence these properties. The factors included were the major chemical constituents dissolved in the aqueous solution, aluminate concentration (a minor constituent) in the aqueous solution, w/cm ratio and the ratio of cementitious materials (FA to BFS to PC).

3.1 Degree of Hydration – Low Aluminate Case

The measurements of the heats of hydration for the individual components of the premix in the MCU solution at a 0.60 w/cm ratio and 0.05 M aluminate (see Table 2-2) are presented in Figure 3-1. These data reveal that with either PC or BFS in MCU solution, the normalized heat (J/g of

cm) produced as a result of hydration is ~ 350 J/g while the normalized heat for the Class F fly ash in MCU solution (at 0.05 M aluminate) is significantly less (~ 70 J/g) after 50 days.

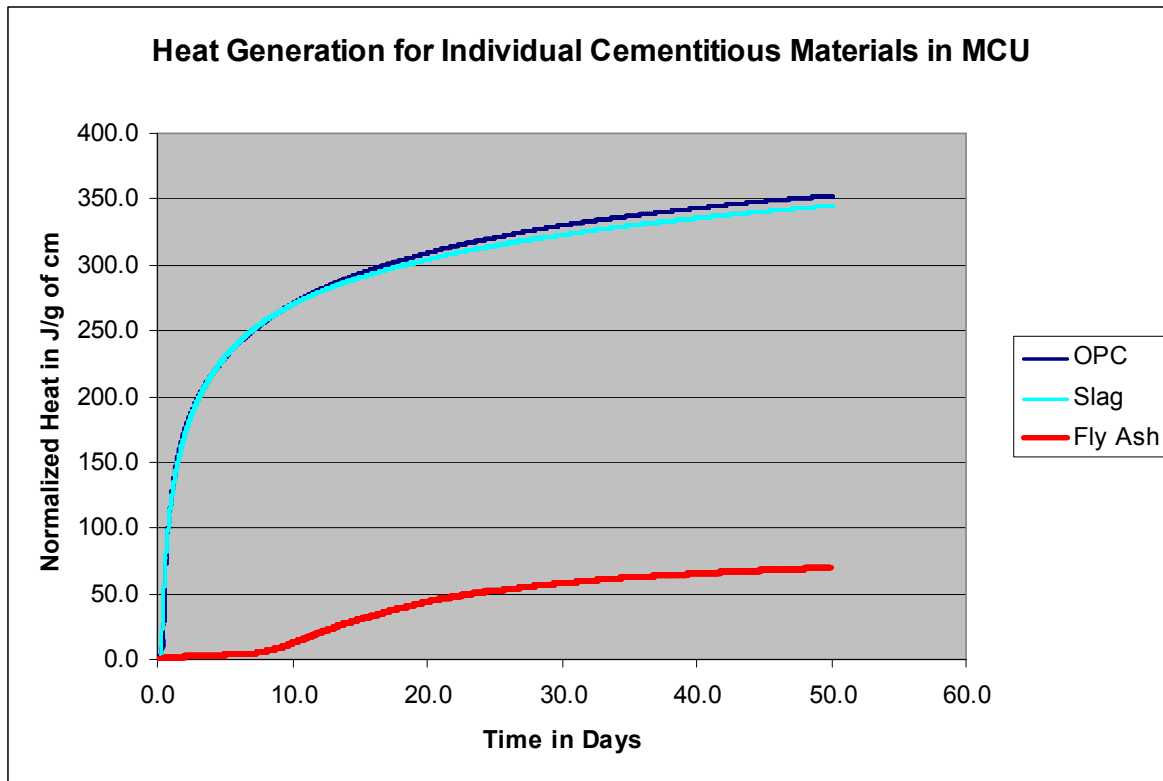


Figure 3-1 Normalized heat generation for each of the cementitious components of the premix in MCU simulant at a 0.60 w/cm ratio.

Typically, the heat generation for complete hydration of Type I/II portland cements in water is on the order of 400 J/g. In a control experiment, the measured value for the heat of hydration for the Type II portland cement used in this study in water was ~ 400 J/g at 28 days at 25 °C. Therefore, the degree of hydration of the portland cement (assuming that 400 J/g reflects 100 % hydration) has been reduced by ~ 12 % in the MCU salt solution relative to water (i.e., the hydration reactions reach only ~ 88 % of the hydration capacity of PC in water).

Blast furnace slag hydration is dependent on the concentration of alkali in the solution (see Section 3-2). Using a 4.0 M NaOH liquid, the normalized heat of hydration was ~ 395 J/g at 40 days for BFS at 0.60 w/cm ratio. The rate of hydration of BFS at 25 °C is slower than the rate of PC hydration under similar conditions, and consequently, the hydration of BFS had not leveled off by 40 days. Therefore, the projected level of hydration for BFS in the NaOH solution was estimated at 410 J/g of BFS. Based upon a value of 410 J/g of cm for complete hydration, the degree of hydration of BFS was reduced by ~ 15 % in the MCU salt solution relative to water (i.e., the hydration reactions reached ~ 85 % of the hydration capacity of BFS in 4.0 M NaOH).

As was the case with BFS, the Class F fly ash hydration is dependent on alkali concentration in the solution for activation. Schindler [16, 17] has proposed that the maximum heat generation of

FA is dependent on the calcium content in the FA. For example Schindler has calculated that a Class F fly ash containing 10.8 wt % CaO has a maximum heat generation of 194 J/g of FA for 100 % degree of hydration. The CaO content of the Class F Fly ash used in the current study is ~ 1.1 wt % which leads to a predicted heat of hydration value of ~ 22 J/g of fly ash [17]. A calorimetric measurement was carried out using Class F FA in 4.0 M NaOH and a value of 70 J/g of FA was determined. The lack of complete hydration of the FA is shown in Figure 3-2 which is a back scattered electron (BSE) scanning electron microscope (SEM) image of a polished sample from an MCU mix at 0.65 w/cm ratio. This image shows unreacted fly ash and confirmed by EDS compositional measurements.

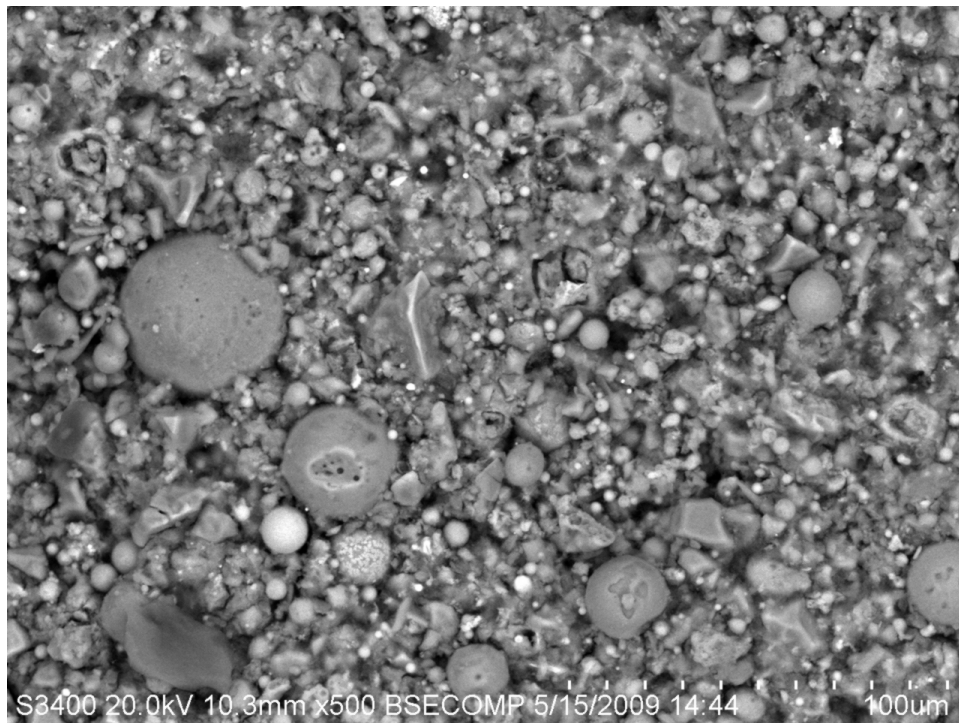


Figure 3-2 A BSE image of a polished cured paste sample batched at 0.65 w/cm ratio with an MCU simulant.

Therefore, a determination of 100 % degree of hydration of FA under these conditions is complicated. We selected a value of 70 J/g of FA as a measure of complete hydration for this set of conditions.

Using the simple law of mixtures [18], one can calculate the projected heat of hydration of the mix of cementitious materials containing 45 wt % BFS, 45 wt % FA and 10 wt % PC. The values of hydration used for the individual cementitious materials were the individual curves shown in Figure 3-1. This time dependent calculated curve is presented in Figure 3-3 along with the measured heat of hydration for this premix in MCU solution at 0.60 w/cm ratio. The actual heat generation is ~ 35 % less than that predicted curve based on the assumption that each component of the premix hydrates independently of the other components. Since the degree of

reaction is related to the performance properties of the mixes, this reduction in degree of reaction in turn reduces the performance properties of the Saltstone paste.

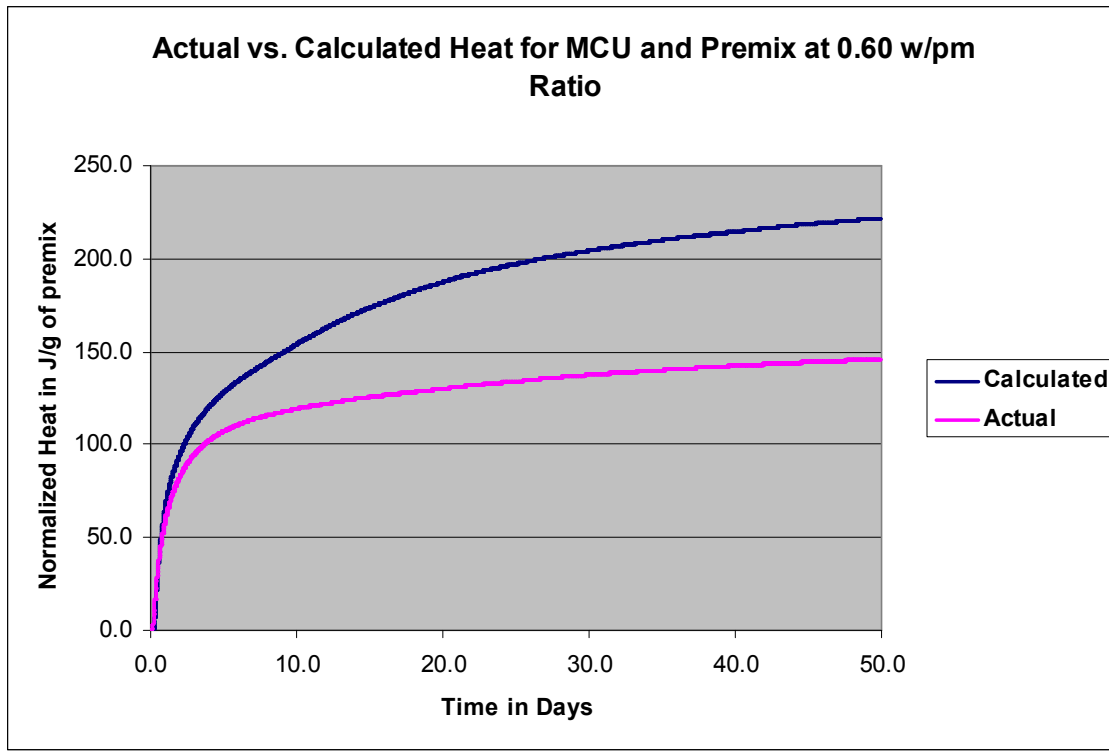


Figure 3-3 Actual vs. calculated normalized heat generation for the premix in MCU at 0.60 w/pm ratio

In an effort to understand the interaction between the cementitious components that leads to less hydration with the premix than predicted, a series of three experiments was carried out as detailed in Table 3-2. In this series of three tests, mixes of (1) 50 % PC and 50 % BFS, (2) 50 % PC and 50 % FA, and (3) 50 % BFS and 50 % FA were batched using the MCU simulant at a w/cm ratio of 0.60 with 0.05 M aluminate. The measured 28 day heats of hydration for the individual components at 0.60 w/cm ratio in MCU solution are also provided. The actual and predicted heats of hydration for the 50/50 mixes show that hydration proceeds basically as expected indicating no significant interactions between the components. Consequently, the 35 % reduction in hydration observed in Figure 3-2 appears to reflect complicated interactions between the three cementitious components during hydration. These heats of hydration data in Table 3-1 are for 28 day durations, and the slight differences between the measured and predicted values may also reflect kinetic differences in the hydration reactions. Similar reductions in the degree of hydration with the nominal premix composition were obtained for mixes using the SWPF simulant although the maximum heat output predicted in this case was 230 J/g of cm. This higher maximum value may reflect the higher alkaline content of the SWPF simulant compared to the MCU simulant.

Table 3-1 Measured and Predicted 28-Day Normalized Heats of Hydration for the 3 Mixes in MCU Solution at a Water to Cementitious Materials Ratio of 0.60.

Cementitious Material			28 Day Heat of Hydration (J/g)	
OPC (%)	BFS (%)	FA (%)	Measured	Predicted
0	50	50	187	183
50	0	50	192	186
50	50	0	314	324
100	0	0	327	NA
0	100	0	320	NA
0	0	100	56	NA

3.2 Alkali Activation of Blast Furnace Slag and Class F Fly Ash

Sodium hydroxide in the aqueous salt solutions activates the hydration reactions of the powdered BFS [5]. The concentration of sodium hydroxide in the radioactive salt solutions is projected (with variation in feed streams within the MCU and SWPF processes) to range roughly from 1 to 3.5 M. The actual NaOH concentration in a given waste stream will be a factor in determining the degree of hydration and consequently the performance properties of the cured grouts. Figure 3-3 shows the dependence of the heat of hydration of BFS used at the SPF on the concentration of sodium hydroxide in the aqueous solution. At 4 M NaOH the heat generation approaches 400 J/g of BFS at 40 days while at 1.0 M NaOH, the heat generation approaches 165 J/g after 40 days.

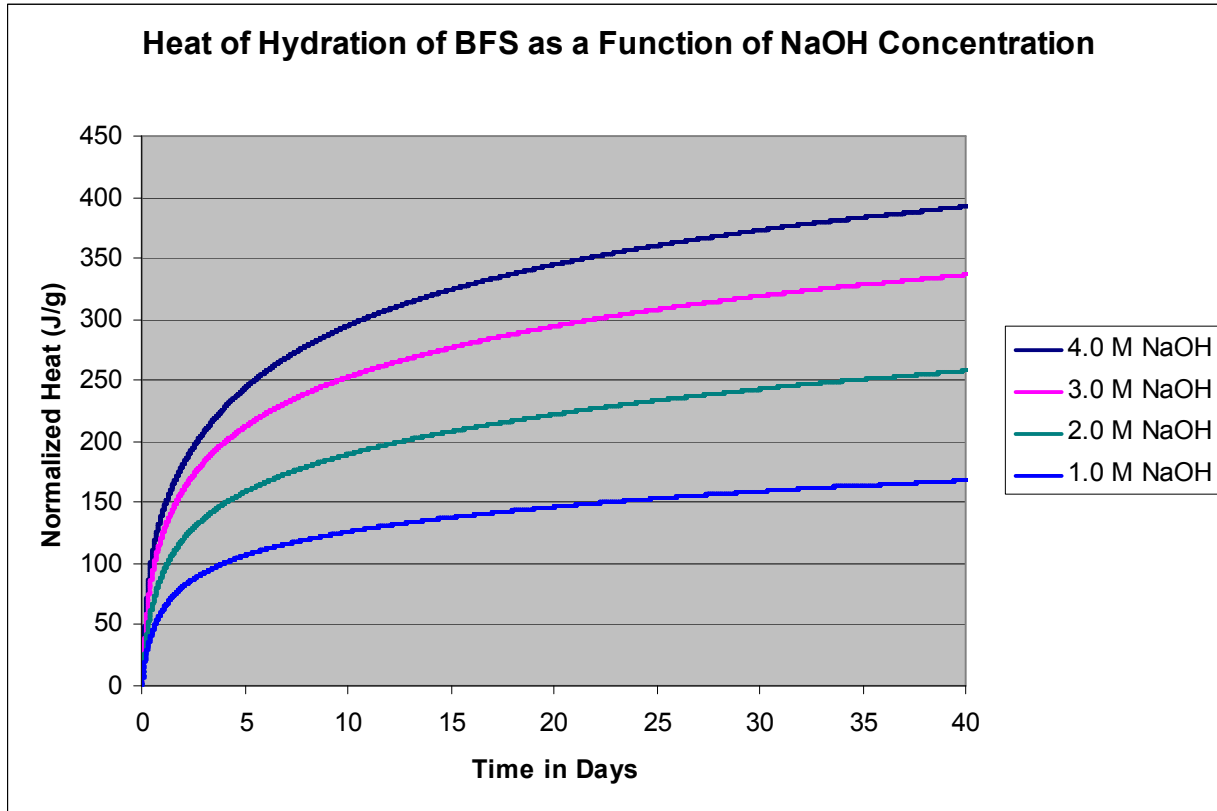


Figure 3-4 Heat of hydration for blast furnace slag as a function of NaOH molarity at 0.60 w/cm ratio

Class F Fly Ash is also activated by NaOH and heat production reaches a value of 59 J/g for a solution which is 3.0 M NaOH at 28 days. This value is essentially equivalent to that observed with the fly ash in the MCU salt solution after 28 days (Figure 3-1). Therefore both the BFS and FA in the MCU solution reach a heat production per gram of cementitious material that is only reached in NaOH solutions at 3.0 M. This suggests that other salts present in the simulated salt solutions may enhance the degree of hydration.

3.3 Impact of Aluminate on Degree of Hydration

The impact of aluminate on degree of hydration as reflected in the heat of hydration and performance property data is revealed by the results of testing on two MCU mixes with different aluminate concentrations under the same w/cm ratio and premix distribution of 45 wt % FA, 45 wt % BFS and 10 wt % PC (Figure 3-5). With the higher level of aluminate (in this case 0.28 M) there is an initial induction period that lasts from 4 to 5 days. This induction period is also reflected in the set time of 5 to 6 days as measured using the Vicat consistency tester. However, once the induction period is over, the heat generation from the hydration reactions in the higher aluminate simulant quickly overtakes the heat generation of the mix with a 0.05 M aluminate

concentration. At 30 days, the heat produced from the 0.05 M aluminate mix is ~35 % lower than the heat generated by the mix with 0.28 M aluminate.

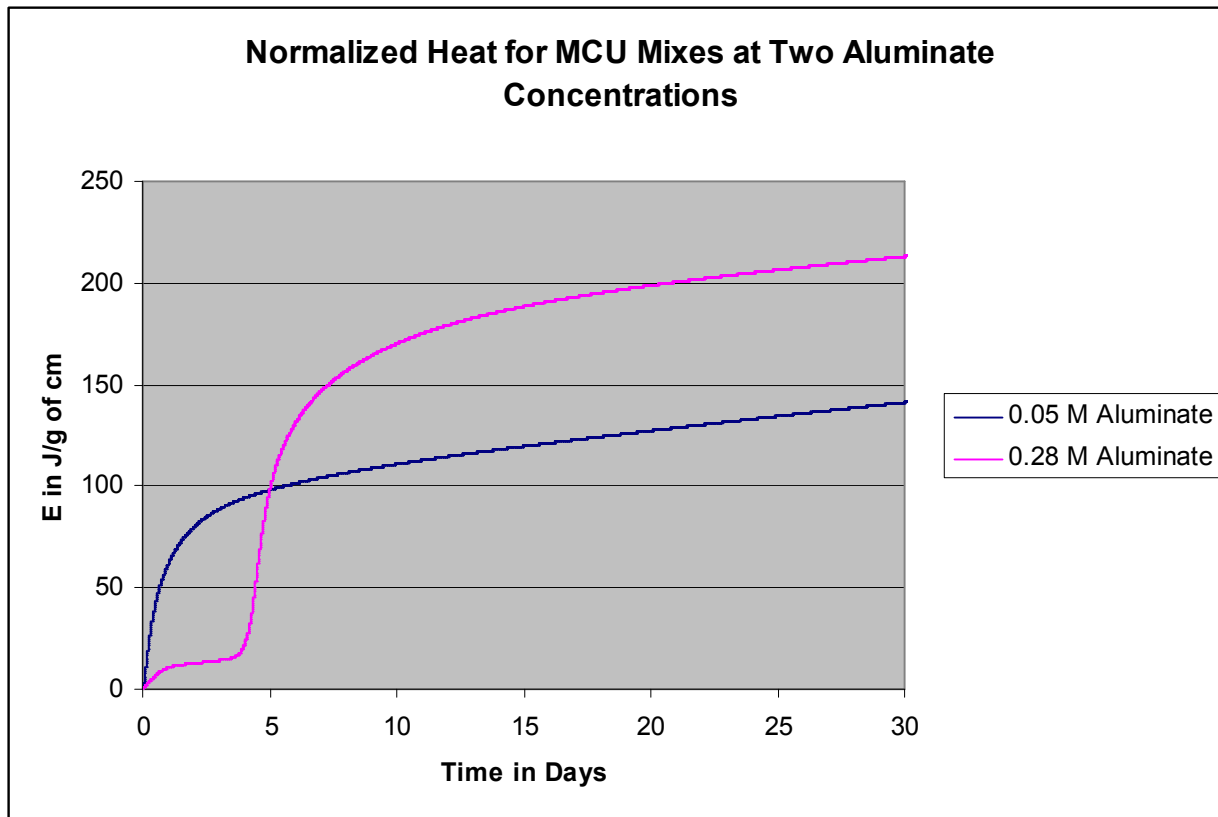


Figure 3-5 Normalized heat production for ARP/MCU mixes at two different aluminate concentrations at 0.60 w/cm ratio

Mixes batched with SWPF simulants show the same general trend observed with the MCU mixes for the impact of aluminate on degree of hydration (Table 3-2). SWPF simulants were prepared with low and high aluminate levels and batched with the nominal premix composition at 0.60 w/cm ratio. The mix with the 0.449 M aluminate had higher values of Young’s modulus, compressive strength and heat of hydration and a lower value of total porosity implying that increased levels of aluminate in the SWPF salt solution improve the overall performance properties of the grout mixes.

Table 3-2 Properties of Two SWPF Mixes at Different Aluminate Concentrations

Aluminate M	Simulant	E at 20°C Gpa	Porosity at 20°C %	Compressive Strength MPa	Heat of Hydration J/g of cm
0.114	SWPF	6.88	61.1	6.4	175
0.449	SWPF	9.47	58.2	16.4	230

The mechanism for this increased degree of hydration can be associated with the aluminate ion concentration in the salt simulants. The initial impact of higher concentrations of aluminate ions in the salt solutions is to retard hydration which leads to a relatively long induction period in the heat of hydration. The length of time of this induction period depends not only on the concentration of aluminate but also on other factors including the types and concentrations of salt in the solution, the w/cm ratio, and the ratios of cementitious materials. Mehta [19] has suggested that dissolved aluminate can react with silicate on the surface of BFS to form a temporary barrier of aluminosilicate that prevents further hydration reactions. Previous work [14] has shown that the induction period in the MCU and SWPF mixes is associated with the BFS (rather than the PC or FA) and the aluminate.

After the induction period, the hydration reactions are activated and reach the predicted degree of hydration (rather than the experimental value) shown in Figure 3-1. It is the presence of aluminate ions in the salt solutions that enables the hydration reactions to reach full potential. Therefore, the aluminate ions play a dual role in these systems by initially retarding hydration and subsequently enabling the hydration reactions. Table 3-3 presents the aluminum contributions from all sources of an MCU mix at 0.60 w/cm ratio, a normal distribution of cementitious materials and a 0.22 M aluminate level.

Table 3-3 Aluminum Contribution from an MCU Mix at 0.60 w/cm Ratio, a Normal Distribution of Cementitious Materials and an Aluminate Concentration of 0.22 M

Source	Aluminum g / 1000 g mix	% of Mix
Simulant	2.16	4.28
BFS	10.38	20.59
FA	36.32	72.03
PC	1.56	3.09
Total	50.42	100.00

Using nuclear magnetic resonance techniques, it has been shown that aluminum is introduced into the CSH in a bridging position but can also be incorporated in other phases [7-8]. Samples of the cured paste were therefore examined with qualitative XRD to determine whether there was evidence for any crystalline aluminum containing species. SWPF mixes with 100 % BFS showed evidence of magnesium aluminum hydroxide hydrate, $Mg_6Al_2(OH)_{18} \cdot 4.5H_2O$. This set of peaks was also present in SWPF mixes with the normal premix both at 0.11 M and 0.33 M aluminate. SWPF mixes with 100 wt % portland cement did not show this species.

3.4 Young's Modulus as a Function of w/cm Ratio and Wt % Slag

As previously discussed, there is an increase in Young's modulus (and degree of hydration) for samples with higher levels of aluminate. Typically, the value of E is between 6 to 7 GPa for mixes containing low levels of aluminate. Due to the projected addition of aluminate to the SWPF stream, a simulant was chosen for Phase 2 that contained 0.28 M aluminate versus the originally projected 0.11 M aluminate. The values of E for 8 of the 10 SWPF mixes of Phase 2

(GVS 98- GVS 105) as a function of w/cm ratio at two different BFS loadings are presented in Figure 3-6. The samples were cured under sealed conditions at room temperature (22 °C). It is clear from these data that decreasing the w/cm ratio from 0.65 to 0.50 increases Young's modulus by ~ 25 % independent of the slag loading. The second conclusion that can be drawn from these data is that an increase in wt % BFS from 45 to 60 wt % in the mix of cementitious materials at the expense of FA increases E by ~ 12 %. Therefore, by reducing the w/cm ratio and/or increasing the wt % BFS in the premix, an improvement in performance as measured by E can be achieved for the cured samples.

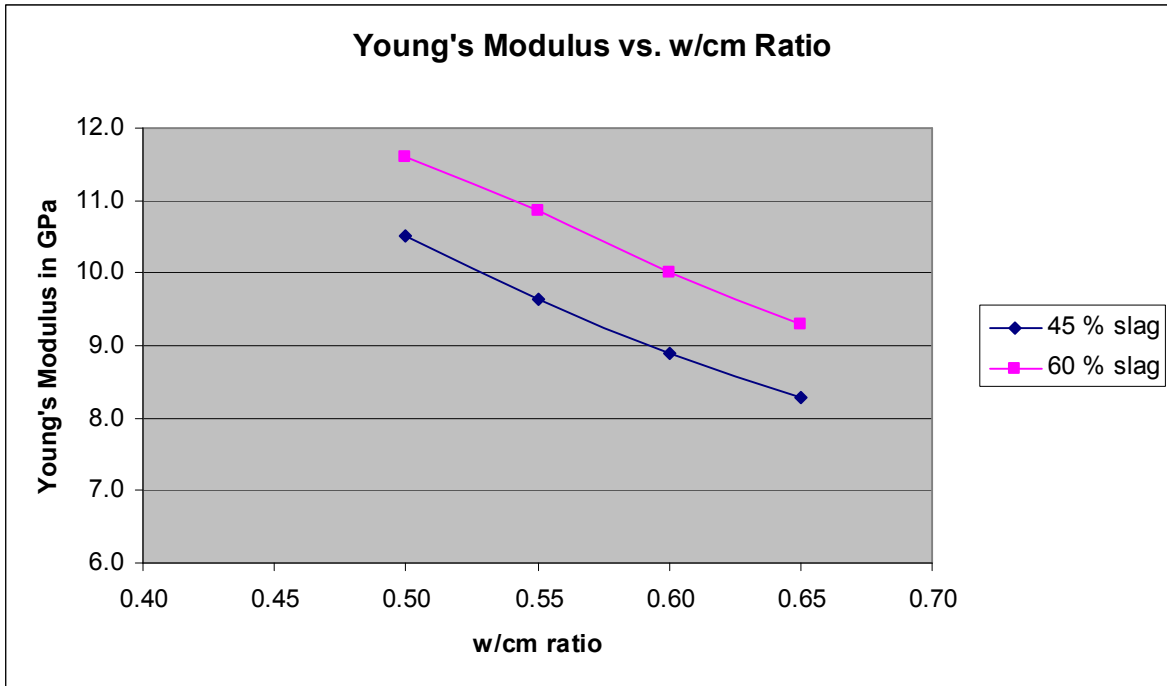


Figure 3-6 Young's modulus (E) values for eight SWPF mixes as a function of w/cm ratio and wt % slag for samples cured at 22 °C for 28 days

The total porosities (Φ) for these 8 mixes were also measured. The total porosity values (expressed as fractions) for samples cured at 22 °C are shown in Figure 3-7. The total porosity decreases with (1) decreasing w/cm ratio and (2) increasing BFS content. This is consistent with the trend of E values for these same mixes as shown in Figure 3-6.

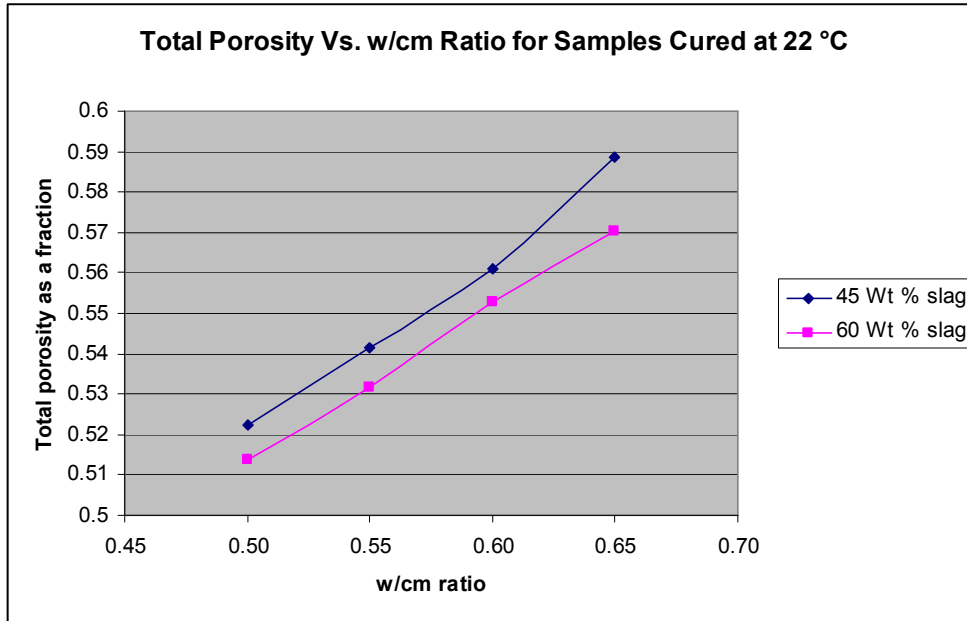


Figure 3-7 Total porosities for mixes batched with either 45 or 60 wt % slag as a function of w/cm ratio. Porosities were measured after 28 days of curing at 22 °C.

3.5 Heat of Hydration

The heat of hydration data for Phase 1 and 2 mixes are provided in Table 3-4. As the w/cm ratio increases for the Phase 2 mixes at both 45 and 60 wt % slag concentrations, the heat of hydration normalized to the premix content actually increases. This is most likely due to the facts that (1) there is a better dispersion of the cementitious particles in grouts with higher water content and (2) there is more water available for hydration at higher water content. However, the heat of hydration, normalized to the mass of grout is essentially the same for the set of four mixes with 45 wt % slag at 125 J/g and for the same set of four mixes with 60 wt % slag at 151 J/g of Phase 2. The difference in heat generation between these two sets is mainly due to the differences in slag content. The model developed and discussed in Section 3.7 of this report details the dependence of heat of hydration on all significant factors for the combined 1 and 2 phases.

Table 3-4 Normalized Heat of Hydration for Phases 1 and 2 Mixes

Identifier	Heat	Heat Flow
	J/g of cm	peak time (hours)
GVS87	240	43
GVS88	174	10
GVS89	187	7
GVS90	221	3
GVS91	226	44
GVS92	216	4
GVS93	299	39
GVS94	229	49
GVS95	258	61
GVS96	235	39
GVS98	210	54
GVS99	220	54
GVS100	230	58
GVS101	239	51
GVS102	256	27
GVS103	270	30
GVS104	277	33
GVS105	286	35

3.6 Processing Properties

This report has focused mainly on the performance properties of the Saltstone mixes. However, the processing properties must also be acceptable for processing, transfer and placement of the Saltstone within the vaults at the SPF. The processing property results for Phases 1 and 2 mixes are presented in Table 3-5. Two of the mixes had relatively high yield stress and plastic viscosity values. These mixes had a 0.50 w/cm ratio and 60 wt % slag which are mixes at the extreme of the variation window investigated. Normally, the w/cm ratio is and will be as high as acceptable for processing and performance in order to increase the loading of radioactive salt solution into the Saltstone. Pumping calculations will be performed to determine the limits on the rheological properties to ensure proper placement. The set times, bleed volumes and densities are all acceptable for processing these mixes.

Table 3-5 Processing Properties for Phase 1 and 2 Mixes

Identifier	Fresh Density	Yield Stress	Viscosity	Bleed	Set Time
	g/mL	Pa	mPa s	Vol %	Days
GVS87	1.76	4.2	112	0.7	3
GVS88	1.72	3.0	72	2.4	1
GVS89	1.79	6.6	186	0.0	1
GVS90	1.74	5.7	95	0.0	1
GVS91	1.78	6.6	194	0.0	2
GVS92	1.84	15.8	216	0.0	1
GVS93	1.76	3.4	86	0.0	2
GVS94	1.71	3.4	71	0.7	3
GVS95	1.80	7.7	161	0.0	3
GVS96	1.77	5.2	111	0.2	3
GVS97	1.74	4.6	124	0.5	2
GVS98	1.77	7.9	203	0.0	2
GVS99	1.76	5.0	128	0.5	3
GVS100	1.71	3.6	95	0.6	3
GVS101	1.71	2.2	53	0.5	3
GVS102	1.84	10.5	182	0.0	2
GVS103	1.77	6.6	118	0.0	2
GVS104	1.74	4.6	79	0.3	2
GVS105	1.71	3.3	58	0.3	2
GVS106	1.74	5.6	108	0.0	2

3.7 Predictive Models

One objective of this work was to determine which operational and compositional factors are important in determining the values of physical properties (responses) of the Saltstone mixes. In this section of the report, the results of empirical models for Young’s modulus, total porosity and heat of hydration are presented. In this report only linear models (using JMP Version 7.02) [20] were investigated with data limited to Phase 1 and 2 mixes as detailed in Section 2.2, Experimental Design.

For Young’s modulus, the predicted versus actual values are plotted and generate a linear fit with an R^2 equal to 85 % (Figure 3-8). The data points used for this prediction include 20 mixes from Phases 1 and 2. This initial set of 20 mixes will serve as the basis to which additional data from future mixes will be added. The models will be revised as new data are added.

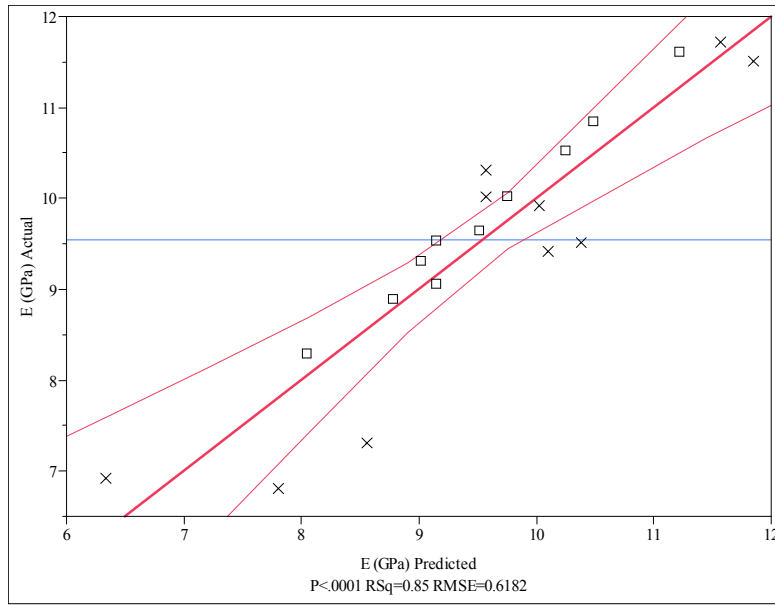


Figure 3-8 Actual versus predicted values of Young’s modulus for samples of Phases 1 and 2 including results for samples cured at different temperatures

The model (equation) for prediction of E, where [] indicates molarity is:

$$E \text{ (GPa)} = 15.40 - 14.68 \cdot w/cm + 0.07 \cdot \text{wt \% BFS} + 8.37 \cdot [\text{aluminate}] - 1.25 \cdot [\text{nitrate} + \text{nitrite}]$$

Thus, the factors that are statistically significant for prediction of E are w/cm ratio, wt % BFS, aluminate molarity and total nitrate + nitrite molarity.

For total porosity, the predicted versus actual values are plotted and provide a linear fit with an R² equal to 76 % (Figure 3-9). These data points are for Phases 1 and 2.

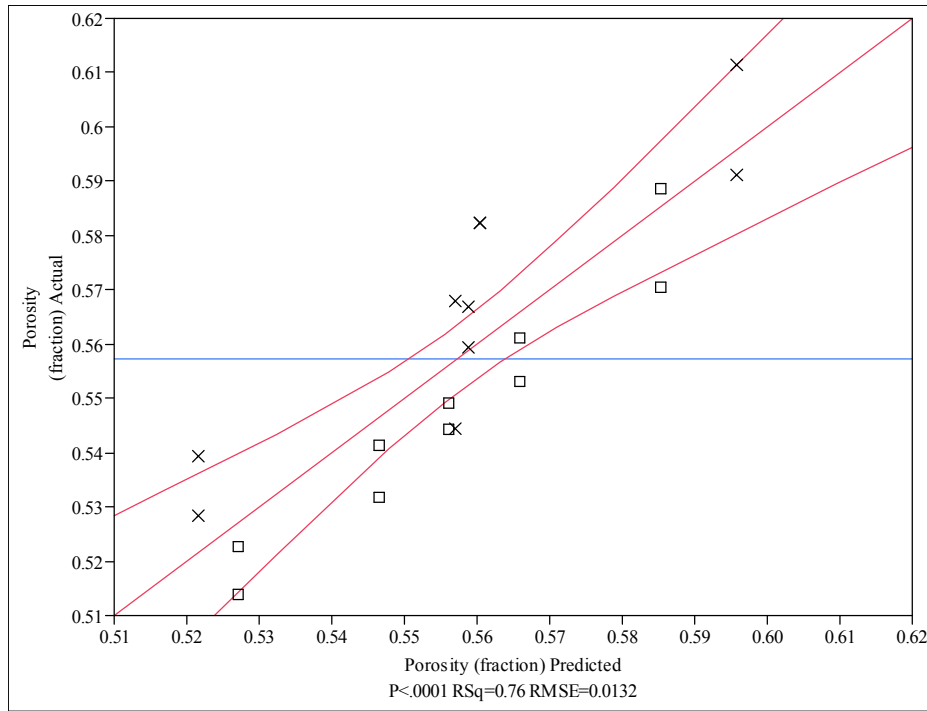


Figure 3-9 Actual vs. predicted values of total porosity for samples of Phases 1 and 2

The model for prediction of total porosity (Φ) expressed as a fraction, where [] indicates molarity is:

$$\Phi = 0.25 + 0.39 \cdot w/cm + 0.035 \cdot [\text{nitrate} + \text{nitrite}]$$

Since Young's modulus and total porosity are inversely correlated, the coefficients in the models are of opposite sign for these two properties. Interestingly, aluminate concentration is not a statistically significant factor in the model for porosity over this compositional range but does play a role in the value of E. A general trend of E with Φ has been demonstrated in general for pastes [21-22] and several non-linear empirical equations have been introduced for this correlation [9, 23-24]. We are currently investigating the application of these models to Saltstone pastes which contain close to 6 M Na ions in the initial salt solution and in the final pore solution.

The heat of hydration in J/g of cm was also modeled and the results are provided in Figure 3-10.

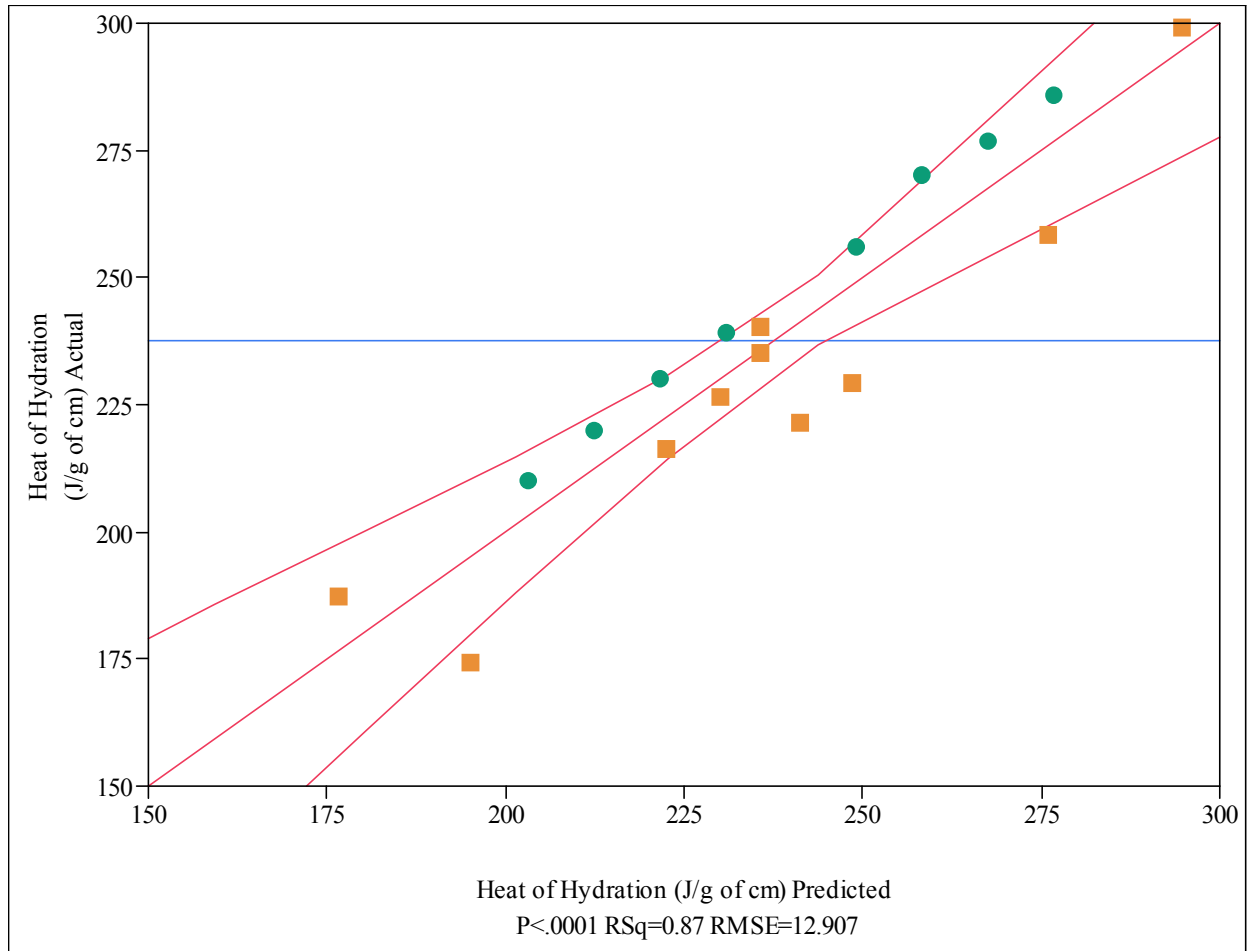


Figure 3-10 Actual vs. predicted values of heat of hydration for samples of Phases 1 and 2 measured at 25 °C. The green circles are data from phase 2 mixes and the orange squares from phase 1 mixes

The model for prediction of heat of hydration (heat) expressed in J/g of cm, where [] indicates molarity is:

$$\text{Heat (J/g of cm)} = -72.86 + 185.69 \cdot w/cm + 3.07 \cdot \text{wt \% BFS} + 159.99 \cdot [\text{aluminate}]$$

The R^2 for this fit is 87 % and identifies w/cm ratio, wt % BFS and aluminate as significant drivers of the heat of hydration normalized to the mass of cementitious materials of the Saltstone mixes.

4.0 CONCLUSIONS

When highly concentrated, alkaline salt solutions containing low levels of aluminate (< 0.1 M) are mixed with a blend of BFS, FA and PC, the resultant paste has a degree of hydration that is only 65 % of the expected value if the individual cementitious materials hydrated independently.

However, an increase in the aluminate concentration in these salt solutions to levels between 0.22 and 0.44 M, results in pastes with the expected degree of hydration. The higher degree of hydration in turn leads to improved performance properties of the Saltstone pastes, a result which decreases the release of radionuclides into the environment. However, even at these expected levels of hydration, the fly ash has not reacted to a significant degree as has been observed through isothermal calorimetry and electron microscopy.

For a fixed simulant, measurements of dynamic Young's modulus, total porosity, compressive strength and heat of hydration reveal that performance properties are improved by increasing the wt % of BFS at the expense of FA in the blended cementitious mix and by decreasing the w/cm ratio of the paste. For the results from mixes of both phases 1 and 2, empirical models (based on a linear fit of the data) were developed that identified the factors that are statistically significant in predicting, heat of hydration, total porosity and dynamic Young's modulus. These factors included the concentrations of aluminate, free hydroxide and total sodium nitrate plus nitrite salts in the solutions.

5.0 REFERENCES

- (1) K. H. Rosenberger, B. C. Rogers, and R. K. Cauthen, Saltstone Performance Objective Demonstration Document, CBU-PIT-2005-00146 Rev 0, June 2005.
- (2) C. A. Langton, M. D. Dukes and R. V. Simmons, Cement-Based Waste Forms for Disposal of Savannah River Plant Low-Level Radioactive Salt Waste, Scientific Basis for Nuclear Waste Management VII, p. 575–582, Proceedings of the Materials Research Society Annual Meeting, Boston, MA, November, 1983.
- (3) I.G. Richardson, Tobermorite/Jennite and Tobermorite/Calcium Hydroxide-based Models for the Structure of C-S-H: Applicability to Hardened Pastes of Tricalcium Silicate, β -Dicalcium Silicate, Portland cement, and Blends of Portland Cement with Blast-Furnace Slag, Metakaolin, or Silica Fume, Cement and Concrete Research, 34, 1733–1777, 2004.
- (4) A. Nonat, The structure and stoichiometry of C-S-H, Cement and Concrete Research, 34, 1521–1528, 2004.
- (5) C. Shi and R. L. Day, Some Factors Affecting Early Hydration of Alkali-Slag Cements, Cement and Concrete Research, 26, 439-447, 1996.
- (6) J. C. Kim and S. Y Hong, Liquid Concentration Changes During Slag Cement Hydration by Alkali Activation, Cement and Concrete Research, 31, 283-285, 2001.
- (7) S-D Wang and K. L. Scrivener, ^{29}Si and ^{27}Al NMR Study of Alkali-Activated Slag, Cement and Concrete Research, 33, 769–774, 2003.

- (8) J. Schneider, M.A. Cincotto, H. Panepucci, 29Si and 27Al High-Resolution NMR Characterization of Calcium Silicate Hydrate Phases in Activated Blast-Furnace Slag Pastes, Cement and Concrete Research, 331, 993–1001, 2001.
- (9) H. F. W. Taylor, Cement Chemistry, Thomas Elford Publishing, London, 2004.
- (10) J. Davidovits, D. C. Comrie, J. H. Paterson, and D. J. Ritcey, Geopolymeric Concretes for Environmental Protection, Concr. Int., 1990, 30-40, 1990.
- (11) J. W. Phair and J. S. J. van Deventer, Characterization of Fly-Ash-Based Geopolymeric Binders Activated with Sodium Aluminate, Ind. Eng. Chem. Res. 2002, 41, 4242-4251 (2002)
- (12) D. J. McCabe, R. A. Peterson, J. A. Pike and W. R. Wilmarth, Aluminum and Chromium Leaching Workshop Whitepaper, WSRC-STI-2007-00168, 2007.
- (13) R. O. Lokken, Effect of Aluminate Ions on the Heat of Hydration of Cementitious Waste Forms, PNL-SA-22330, Pacific Rim Conference, Honolulu (1993).
- (14) J. R. Harbour, T. B. Edwards, E. K. Hansen and V. J. Williams, Impact of Aluminate Ions on the Properties of Saltstone Grout Mixes, Proceedings of the Self-Consolidating Concrete Conference, Chicago, 2008
- (15) R. E. Eibling, E. K. Hansen and B. R. Pickenheim, Potential Impact of Blending Residual Solids from Tanks 18/19 Mounds with Tank 7 Operations, WSRC-STI-2007-00113 Revision 0, 2007.
- [16] A. K. Schindler, Effect of Temperature on Hydration of Cementitious Materials, ACI Materials Journal, 101, 1, 73-81, (2004)
- [17] A. K. Schindler and K. J. Folliard, Heat of Hydration Models for Cementitious Materials, ACI Materials Journal, 102, 1, 24-33 (2005)
- (18) D. P. Bentz, Transient Plane Source Measurements of the Thermal Properties of Hydrating Cement Pastes, Materials and Structures, 40, 2007.
- (19) P. K. Mehta, Pozzolonic and Cementitious By-Products in Concrete – Another Look, Proceedings of the 3rd International Conference on Fly Ash, Silica Fume, Natural Pozzolons in Concrete, Trondheim, Norway, pages 1-43, 1989.
- (20) JMP Version 7.0.2, SAS Institute, Inc. Cary, NC, 1989-2007
- (21) G. W. Scherer, J. J. V. II, and G. Simmons, New Methods to Measure Liquid Permeability in Porous Materials, Cement and Concrete Research, 37, 386–397, (2007).
- (22) W. Vichit-Vadakan and G. W. Scherer, Measuring Permeability of Rigid Materials by a Beam-Bending Method: III, Cement Paste, J. Am. Ceram. Soc., 85 [6], 1537–44 2002.

(23) R. A. Helmuth and D. H. Turk, J. PCA Res. Dev. Labs, 9 (2) 8 (1967).

(24) S. Kamali, M. Moranville, E. Garboczi, S. Prené, and B. Gérard, Hydrate Dissolution Influence on the Young's Modulus of Cement Pastes, Proceedings of the International Conference on Fracture Mechanics of Concrete and Concrete Structures (2003).